JOURNAL OF GEOPHYSICAL RESEARCH: SOLID EARTH, VOL. 118, 1837–1844, doi:10.1002/jgrb.50145, 2013

Vertical and horizontal surface displacements near Jakobshavn Isbræ driven by melt-induced and dynamic ice loss

Karina Nielsen,[1] Shfaqat A. Khan,[1] Giorgio Spada,[2] John Wahr,[3] Michael Bevis,[4] Lin Liu,[5] and Tonie van Dam[6]

Received 16 August 2012; revised 5 March 2013; accepted 6 March 2013; published 29 April 2013.

[1] We analyze Global Positioning System (GPS) time series of relative vertical and horizontal surface displacements from 2006 to 2012 at four GPS sites located between ∼5 and ∼150 km from the front of Jakobshavn Isbræ (JI) in west Greenland. Horizontal displacements during 2006–2010 at KAGA, ILUL, and QEQE, relative to the site AASI, are directed toward north-west, suggesting that the main mass loss signal is located near the frontal portion of JI. The directions of the observed displacements are supported by modeled displacements, derived from NASA's Airborne Topographic Mapper (ATM) surveys of surface elevations from 2006, 2009, and 2010. However, horizontal displacements during 2010–2012 at KAGA and ILUL are directed more towards the west suggesting a change in the spatial distribution of the ice mass loss. In addition, we observe an increase in the uplift rate during 2010–2012 as compared to 2006–2010. The sudden change in vertical and horizontal displacements is due to enhanced melt-induced ice loss in 2010 and 2012.

Citation: Nielsen, K., S. A. Khan, G. Spada, J. Wahr, M. Bevis, L. Liu, and T. van Dam (2013), Vertical and horizontal surface displacements near Jakobshavn Isbræ driven by melt-induced and dynamic ice loss, *J. Geophys. Res. Solid Earth*, *118*, 1837–1844, doi:10.1002/jgrb.50145.

1. Introduction

[2] Jakobshavn Isbræ (JI), located at the west coast of Greenland, is one of the largest outlet glaciers in terms of drainage basin area. It has been losing mass at a rate of between 25 and 34 Gt/yr since the end of 2002 [*Howat et al.*, 2011]. This loss represents approximately 10% of Greenland's total ice loss [*Jacob et al.*, 2012]. The present-day unloading of ice causes the Earth to respond elastically, resulting in both vertical and horizontal displacement of the crust. The magnitude of this displacement is proportional to the size of the load and inversely proportional to the distance between the load and the observing point. The direction of the deformation depends on the sign of the load; unloading causes uplift and horizontal motion away from the load. To date, primarily the vertical component has been used to study deformations related to present-day ice mass changes in Greenland.

[3] Currently, more than 55 GPS receivers are located around the edge of the Greenland ice sheet. These instruments provide continuous measurements of the 3D surface positions. The majority of these sites are part of the Greenland GPS network (GNET). Here, we use data from four GPS sites (KAGA, ILUL, QEQE, and AASI, Figure 1) to analyze the deformation pattern around JI and thereby understand the nature of the present-day ice loss. A previous study conducted by *Khan et al.* [2010] used GPS measurements from 2006–2009 to study vertical crustal motion near JI. Other studies in Greenland have also used GPS measurements of vertical crustal displacements to study the present ice mass variability [*Khan et al*., 2007; *Bevis et al*., 2012; *Nielsen et al*., 2012] and to constrain the glacial isostatic adjustment (GIA) signal [*Dietrich et al*., 2005; *Khan et al*., 2008; *King et al*., 2010; *Bevis et al*., 2012; *Spada et al*., 2012]. Here, we expand the time series of *Khan et al.* [2010] with an additional 3 years of data, and analyze both vertical and horizontal GPS displacements.

[4] The crustal displacements around JI can be divided into three primary contributions: the Earth's elastic response owing to present-day ice mass loss from JI; the elastic response as a result of ice mass loss outside JI; and GIA, i.e., the Earth's viscoelastic response to past glacial changes. To study present-day ice mass loss within JI, we analyze displacements relative to the station AASI. Forming relative

[1]DTU Space - National Space Institute, Department of Geodesy, Technical University of Denmark, Kgs. Lyngby, Denmark.
[2]Dipartimento di Scienze di Base e Fondamenti (DiSBeF), Università di Urbino "Carlo Bo", Urbino, Italy.
[3]Department of Physics and Cooperative Institute for Research in Environmental Sciences, University of Colorado, Boulder, Colorado, USA.
[4]School of Earth Sciences, Ohio State University, Columbus, Ohio, USA.
[5]Department of Geophysics, Stanford University, Stanford, California, USA.
[6]University of Luxembourg, Luxembourg, Luxembourg.

Corresponding author: K. Nielsen, DTU Space - National Space Institute, Department of Geodesy, Technical University of Denmark, Elektrovej, bygn. 327, Kgs. Lyngby 2800, Denmark. (karni@space.dtu.dk)

2169-9313/13/10.1002/jgrb.50145

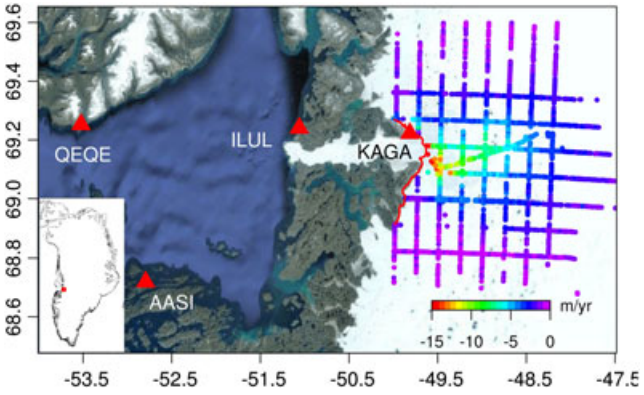

Figure 1. An overview of the area of JI. The red triangles indicate the positions of the four GPS sites. The positions of the ATM tracks and the elevation changes along tracks at 500 m segments (based on ATM data from 2006, 2009, and 2010) are also shown. The red line indicates the 2006 late summer calving front that was acquired from Landsat imagery.

displacements in this way reduces the impact of the present-day signal outside JI and also the impact of the GIA signal. Due to the recent record surface melting events observed in 2010 [*Tedesco et al*., 2011; *Bevis et al*., 2012] and 2012, we divide the analysis into two time periods 2006–2010.4 and 2010.4–2012.

[5] To support this analysis, we model the corresponding displacement field. The modeled rates that are related to the ice mass loss from JI are derived from surface elevation changes based on NASA's airborne topographic mapper (ATM) data for the years 2006, 2009, and 2010 [*Krabill*, 2011]. Displacements outside JI are estimated from an Ice, Cloud, and land Elevation Satellite (ICESat) derived mass change grid that is based on data collected between 2006 and 2009 [*Zwally et al.*, 2010]. We account for the GIA contribution by using the ICE-5G deglaciation history of the late-Pleistocene ice sheets [*Peltier*, 2004].

[6] Additionally, we analyze interannual vertical displacements at each station. By comparing these displacements to the local rates, we distinguish between ice mass loss caused by dynamic thinning and that due to melt-induced ice loss. In general, dynamic thinning is largest near the glacier front (typical values of up to 20 m/yr) and decreases to a few meters per year about 20–30 km upstream. Melt-induced thinning is on the order of a few meters per year near the margin of the Greenland ice sheet and decreases very slowly inland. Consequently, melt-induced thinning normally produces much larger mass changes than dynamic ice loss when large regions are considered [*Van Den Broeke et al.*, 2009].

2. Data and Methods

2.1. GPS Data Analysis

[7] To estimate site coordinates, we follow the procedure of *Khan et al.* [2010]. We use the GIPSY OASIS 6.1.2 software package [*Zumberge et al.*, 1997] developed at the Jet Propulsion Laboratory (JPL), and released in January 2012. The orbit products we use were released in 2012 by JPL and included satellite orbits, satellite clock parameters and Earth orientation parameters. The orbit products take the satellite antenna phase center offsets into account. Receiver clock parameters are modeled, and the atmospheric delay parameters are modeled using the Vienna Mapping Function 1 (VMF1) [*Böhm et al.*, 2006; *Kouba*, 2007]. Corrections are applied to remove the solid Earth tide and ocean tidal loading. The amplitudes and phases of the main ocean tidal loading terms are calculated using the Automatic Loading Provider (http://www.oso.chalmers.se/~loading, *Scherneck and Bos* [2002]) applied to the FES2004 ocean tide model including correction for center of mass motion of the Earth due to the ocean tides. The site coordinates are computed in the ITRF2008 frame [*Altamimi et al.*, 2012]. The secular trends and their uncertainties are estimated as described in *Khan et al.* [2010]. Annual displacement cycles are modeled using a four term Fourier series [*Bevis et al*., 2012].

2.2. Elevation Changes

[8] To estimate elevation changes on JI between 2006 and 2010, we use NASA's ATM laser altimetry data [*Krabill*, 2011] from 2006, 2009, and 2010 (see Figure 1). From these surface elevation data sets, we estimate a linear trend at along-track points with 500 m spacing. To construct an elevation change map of JI, we interpolate the along-track elevation changes onto a grid with a resolution of 1 km × 1 km, using ordinary local neighborhood kriging. We use the 2006 late summer calving front as the boundary of the elevation change grid. Hence, we have not accounted for the possibility of a smaller floating ice tongue. Based on an area of 7700 km^2, we estimate a volume loss rate of 19.1 ± 5.7 km^3/yr (1σ).

[9] The corresponding uncertainty is estimated as the sum of the individual elements in the kriging covariance matrix. Since the considered mass loss is below the equilibrium-line altitude, we use an ice density of 917 kg/m^3 to convert volume loss to mass loss. This results in a mass loss rate of 17.5 ± 5.2 Gt/yr (1σ). The elevation change grid (Figure 2) shows a thinning rate of –15 m/yr near the front, which decreases gradually to approximately –2 m/yr ~80 km upstream.

2.3. Modeled Crustal Displacement

[10] The horizontal displacement for a disc shaped load, as a function of angular distance α from the center of the disc, is given by (see, e.g., *Spada* [2003])

$$V(\alpha) = 3\Delta H\left(\frac{\rho_i}{\rho_e}\right)\sum_{n=0}^{n_{\max}} l_n \frac{\sigma_n}{2n+1}\frac{\partial P_n(\cos\alpha)}{\partial\alpha}, \qquad (1)$$

where ρ_i is the density of ice, ρ_e is the average density of the Earth, ΔH is the ice thickness change, P_n is the Legendre polynomial of degree n, l_n is the nth harmonic component of the horizontal loading deformation coefficient (LDC) [*Farrell*, 1972], and σ_n is the nth harmonic component of the surface load. An expression of σ_n for an axis-symmetric load is found in *Spada et al.* [2011]. Here, we account only for the horizontal displacement $V(\alpha)$. An expression for the vertical displacement $U(\alpha)$ is given by equation (4) in *Spada et al.* [2012]. The vertical and horizontal displacements as a function of angular distance are displayed in Figure 3. These curves represent the response of a disc load with a radius

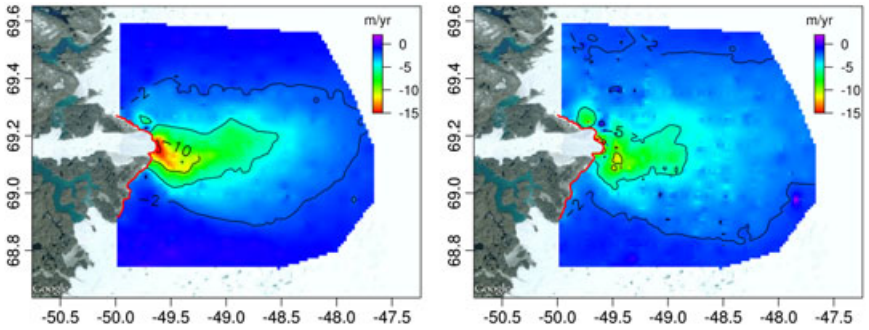

Figure 2. Elevation change grids for JI: (left) Based on ATM data from 2006, 2009, and 2010, the red line indicates the 2006 late summer calving front, acquired from Landsat imagery; (Right) Based on ATM data from 2010–2012, the red line indicates the 2011 late summer calving front.

of 500 m and an ice thickness variation of ΔH = –1 m. The horizontal displacement is largest at the periphery of the load and is zero directly beneath the load due to symmetry. In the case of unloading, the horizontal motion is directed away from the area with mass loss, and towards in case of mass gain. The displacement curves displayed in Figure 3 are based on two different Earth models: first, PREM [*Dziewonski and Anderson*, 1981] and second, the combination of a CRUST2.0-type crust [*Bassin et al.*, 2000] for the area of JI with a REF (or STW105) like mantle [*Kustowski et al.*, 2008]. These models are discussed in more detail below. We refer to this latter Earth model as JAK.

2.3.1. Crustal Displacements Due to Ice Mass Loss From Jakobshavn Isbræ

[11] To model the elastic response due to ice mass loss from JI, we use elastic LDCs based on the Earth model JAK. The crustal characteristics are provided in Table 1. This Earth model has a thicker crust and a lower compressibility in the upper crust compared to the PREM model. These differences influence the displacement pattern in the near field of the source (see Figure 3). The LDCs are estimated by assuming a radially stratified, isotropic and compressible Earth model and they are defined in the Earth's center of mass reference frame. The vertical h and horizontal nl LDCs (up to harmonic degree n = 1024) are displayed in Figure 4 (dashed lines). For higher harmonic degrees, we assume that the asymptotic value of the LDCs is reached. Hence, for $n \to \infty$, the horizontal LDC is $nl_\infty = \frac{\gamma M}{4\pi a^2}\frac{1}{\lambda+\mu}$ [*Farrell*, 1972], where γ is the gravitational acceleration, M and a are the mass and radius of the Earth, λ and μ are the Lamé constants of the uppermost crustal layers.

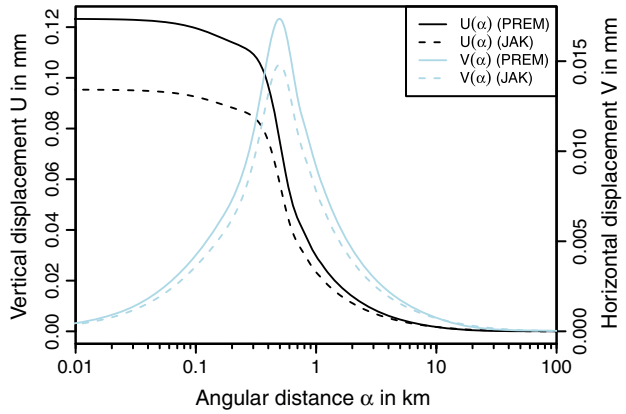

Figure 3. Vertical (black curves) and horizontal (blue curves) displacements in response to a disc load with a radius of 500 m (4.5×10^{-3} degrees) and a thickness variation ΔH = –1 m. The solid curves represent a PREM Earth model, and the dashed curves represent the JAK Earth model (see section 2.3.1). The displacement estimates are calculated by summing up to $n_{max} = 10^5$.

[12] To estimate the crustal displacement caused by the ice mass loss of JI, we transform the mass change grid for JI into a grid of equal area discs. The net crustal displacement at a given location is found by summing the responses from all the individual disc loads. The horizontal component is represented by equation (1). The uncertainty of the modeled displacement rates at an observing point is estimated by propagating the kriging errors from the interpolation of the along-track elevation changes.

2.3.2. Crustal Displacements Due to Ice Mass Loss Outside Jakobshavn Isbræ

[13] The elastic displacements caused by ice mass loss from the Greenland ice sheet outside JI are estimated in the same manner as the local contribution except that a different set of LDCs are used. The LDCs in this estimation are based on an Earth model with PREM structure and are acquired from the Atmospheric pressure loading service (APLO) http://gemini.gsfc.nasa.gov/aplo/. The vertical h and horizontal nl LDCs (up to harmonic degree 1024) are displayed in Figure 4 (solid lines). To represent the mass changes outside JI, we use an ICESat-derived mass change grid based on data from 2006–2009, with a spatial resolution

Table 1. Crustal Characteristics for the CRUST2.0 Type Earth Model for the Area of JI and the APLO PREM Model

Layer	Thickness (km)	v_p (km/s)	v_s (km/s)	ρ (kg/cm^3)
CRUST2.0 type crust for JI				
Ice	0.500	3.810	1.940	0.920
Upper crust	13.000	6.200	3.600	2.800
Middle crust	12.000	6.400	3.600	2.850
Lower crust	12.000	6.800	3.800	2.950
APLO PREM crust				
Crust	15.000	5.800	3.200	2.600
Crust	10.000	6.800	3.900	2.900

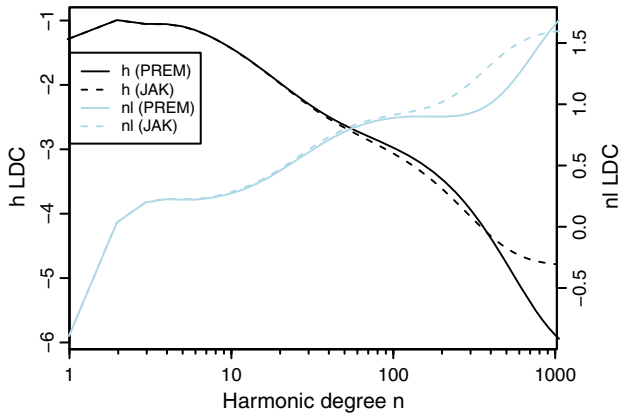

Figure 4. Vertical and horizontal LDCs *h* and *nl* LDCs (up to harmonic degree $n = 1024$) representing a PREM Earth model (solid lines) and the JAK Earth model (dashed lines).

of 5 km× 5 km. The mass change grid is estimated using the method (M3) presented in *Sørensen et al.* [2011]. The time span of this mass change grid is 1.4 years shorter than the JI mass change grid. This difference could contribute an additional error to the estimates of the displacement from the regional mass changes. To quantify this error, we examine the variation in displacements at the GPS sites located near JI from two additional ICESat derived mass change grids based on data from 2004–2007 and 2005–2008. When comparing the absolute displacements at each site, we find a variation range of approximately ± 0.5 mm and ± 0.2 mm for the relative displacements (with AASI as the reference).

[14] We derive a formal error estimate for the displacements due to uncertainties in the 2006–2009 ICESat-derived mass change grid using the bootstrap method, which is a simulation-based statistical analysis. We follow the procedure described in *Sørensen et al.* [2011] that is summarized below. The 2006–2009 elevation change data set consists of *m* tracks. From this data set, we create 1000 new bootstrapped data sets, by randomly drawing *m* tracks with replacements among the tracks in the 2006–2009 elevation change data set. Hence, in the bootstrapped data sets, some tracks might appear more than once. For each bootstrapped data set, we estimate the crustal displacements. The 1000 estimates of crustal displacements form a distribution from which the uncertainty is deduced. If the bootstrap distribution approximates a normal distribution, then $\pm 2\sigma_{\text{boot}}$ represents the 95% confidence interval.

2.3.3. Crustal Displacements Due to GIA

[15] To account for the GIA signal, we use predicted GIA displacement grids based on the deglaciation history ICE-5G(VM2 L90) version 1.3 estimated by W. R. Peltier. The GIA grids are available at http://www.atmosp.physics.

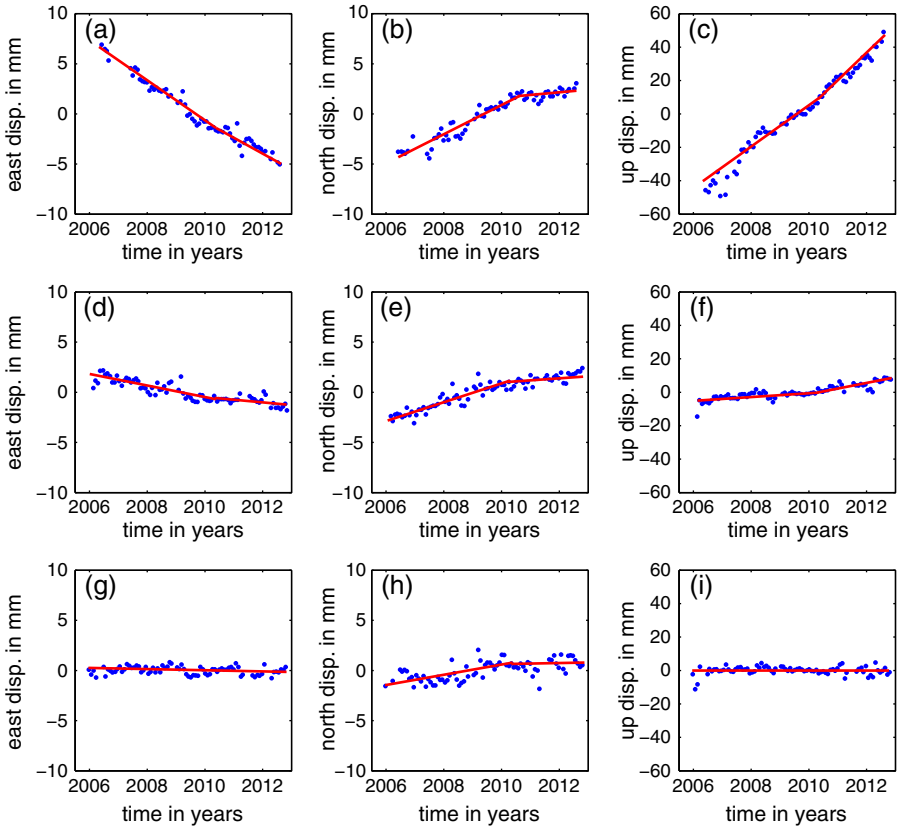

Figure 5. Monthly averages of east, north, and vertical displacements in millimeters relative to AASI. The annual cycle is removed. The red lines show the best fitting linear terms during 2006–2010.4 and 2010.4–2012. (a–c) display relative east, north, and vertical displacements at KAGA, respectively; (d–f) display relative east, north, and vertical displacements at ILUL; (g–h) display relative east, north, and vertical displacements at QEQE. The linear terms and their associated uncertainties are listed in Table 2.

Table 2. Observed and Modeled Vertical and Horizontal Displacements at KAGA, ILUL, and QEQE Relative to AASI[a]

Station	GPS 2006–1010.4	GPS 2010.4–2012	Modeled 2006–2010	Response of JI	Response Outside JI	GIA	
			Vertical component U				
KAGA-AASI	12.3 ± 0.6	14.7 ± 0.4	12.1 ± 2.1	11.5 ± 2.1	1.8 ± 0.4	–1.2	[–1.6; 0.7]
ILUL-AASI	1.2 ± 0.4	2.7 ± 0.4	2.1 ± 0.9	1.7± 0.8	0.9 ± 0.3	–0.5	[–0.8; –0.1]
QEQE-AASI	0.1 ± 0.4	–0.3 ± 0.4	–0.2 ± 0.5	–0.2 ± 0.4	–0.1 ± 0.3	0.1	[–0.3; 0.5]
			East component E				
KAGA-AASI	–2.1 ± 0.2	–1.5 ± 0.2	–2.2 ± 0.5	–3.2 ± 0.5	0.4 ± 0.1	0.6	[0.3; 0.9]
ILUL-AASI	–0.5 ± 0.2	–0.3 ± 0.2	–0.2 ± 0.3	–0.6 ± 0.3	0.0 ± 0.1	0.4	[0.2; 0.6]
QEQE-AASI	0.0 ± 0.2	–0.1 ± 0.2	–0.1 ± 0.1	0.0 ± 0.1	0.1 ± 0.1	–0.2	[0.0; –0.1]
			North component N				
KAGA-AASI	1.5 ± 0.2	0.4 ± 0.2	0.4 ± 0.1	0.6 ± 0.1	0.0 ± 0.1	–0.2	[–0.3; –0.1]
ILUL-AASI	0.9 ± 0.2	0.4 ± 0.2	0.2 ± 0.1	0.3 ± 0.1	0.0 ± 0.1	–0.1	[–0.2; 0.0]
QEQE-AASI	0.4 ± 0.2	0.3 ± 0.2	0.1 ± 0.1	0.2 ± 0.1	–0.1 ± 0.0	0.0	[0.0; 0.1]

[a]The second and third columns display GPS rates; the fourth column shows the total modeled uplift rates that consists of the elastic response from JI (column 5), the elastic response from outside JI (column 6), and GIA (column 7). The GIA estimates are based on ICE-5G(VM2 L90) Version 1.3. All rates are given in millimeter per year. The errors represent one standard deviation σ except for the GIA estimates where ranges are given instead. These ranges represent viscosity variations corresponding to $(0.5 \pm 0.3)\times10^{21}$ Pa s and $(2.7 \pm 0.3)\times10^{21}$ Pa s, for the upper and lower mantles, respectively

utoronto.ca/~peltier/data.php. GIA estimates are sensitive to the viscoelastic structure of the Earth and the deglaciation history.

[16] To assess the variation of GIA estimates due to viscosity, we use an improved version (version 3.2.3) of the software SEa Level EquatioN solver (SELEN) available at http://www.geodynamics.org/cig/software [*Spada and Stocchi*, 2007]. This version accounts for rotational feedback. We approximate the VM2 viscosity profile with a two layer mantle model with an upper and lower mantle viscosity of 0.5 and 2.7 $\times10^{21}$ and let the upper and lower mantle viscosity range between $(0.5 \pm 0.3)\times10^{21}$ Pa s and $(2.7 \pm 0.3)\times10^{21}$ Pa s, respectively. The ranges of the viscosity are chosen such that the agreement of the ICE-5G model with the Holocene relative sea level curves is not altered significantly. Hence, by estimating the GIA contribution within these viscosity limits, we find a range of other possible GIA values.

3. Results

3.1. Relative Displacements

[17] To study horizontal displacements, we consider relative rather than absolute geocentric displacements. Horizontal displacements are dominated by plate motion that is effectively removed by considering relative displacements between sites located relatively close to one another. This approach reduces displacements related to, for example, ice loss outside JI and GIA as these far-field contributions are similar at each GPS site. Thus, the relative rates can be used to validate the local mass balance of JI. The observed displacement rates at KAGA, ILUL, and QEQE (relative to AASI) are displayed in Figure 5, where the blue dots represent monthly averages between 2006 and 2012. The red lines are the best fitting linear terms based on the data between 2006–2010.4 and 2010.4–2012. Figures 5b and 5e show a significant decrease in the northward displacement rate at KAGA and ILUL between 2010.4–2012 compared to 2006–2010.4. This suggests a change in the spatial distribution of the ice mass loss.

[18] The modeled and observed rates of crustal displacement are summarized in Table 2. The discrepancy between the observed and modeled rates is between 0.9 and 0.2 mm/yr for the vertical component, 0.1 and 0.3 mm/yr for the east component, and 1.1 and 0.3 mm/yr for the north component. The vectors in Figure 6 display the direction and amplitude of the horizontal displacements at KAGA, ILUL, and QEQE, relative to AASI. The black and blue arrows represent the observed rates during 2006–2010.4 and 2010.4–2012, respectively. The red arrows represent the modeled rates between 2006 and 2010. The horizontal displacements are generally directed north-west to west-north-west.

3.2. Absolute Vertical Displacements

[19] The modeled and observed absolute vertical rates are summarized in Table 3. Columns 2 and 3 contain observed GPS rates; column 4 contains the total modeled rates that

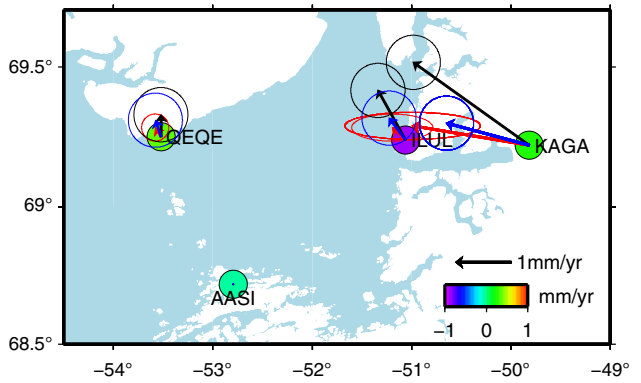

Figure 6. Horizontal displacements relative to AASI observed during 2006–2010.4 (black), observed during 2010.4–2012 (blue), and modeled (red). Contributions to the signal include the elastic response from JI, the elastic response from outside JI, and GIA. The arrows indicate the direction and amplitude of the displacements and the error ellipses indicate the 95% confidence intervals. The colors of the circles represent the offset between the observed and modeled vertical displacements relative to AASI.

Table 3. Modeled and Observed Uplift Rates (in mm/yr) at KAGA, ILUL, QEQE, and AASI[a]

Station	GPS 2006–2012	GPS 2006–2010.4	Modeled 2006–2010	Response of JI	Response outside JI	GIA	
KAGA	21.2 ± 0.6	19.1 ± 0.7	15.5 ± 2.1	12.7 ± 2.1	4.5 ± 0.3	–1.7	[–3.0; 0.5]
ILUL	9.4 ± 0.4	7.7 ± 0.5	5.6 ± 0.7	3.0 ± 0.7	3.6 ± 0.2	–1.0	[–2.2; 1.1]
QEQE	7.7 ± 0.4	6.5 ± 0.5	3.3 ± 0.3	1.1 ± 0.2	2.7 ± 0.2	–0.5	[–1.0; 1.2]
AASI	7.6 ± 0.4	6.2 ± 0.5	3.5 ± 0.4	1.2 ± 0.3	2.7 ± 0.2	–0.4	[–1.4; 1.3]

[a]The second and third columns display GPS rates; the fourth column shows the total modeled uplift rates that consist of the elastic response from JI (column 5), the elastic response from outside JI (column 6), and GIA (column 7). The errors represent one standard deviation σ except for the GIA estimates where ranges are given instead. These ranges represent viscosity variations corresponding to $(0.5 \pm 0.3)\times10^{21}$ Pa s and $(2.7 \pm 0.3)\times10^{21}$ Pa s, for the upper and lower mantles, respectively

includes contributions from elastic displacements related to mass loss from JI, the elastic displacements related to mass loss outside JI, and displacements related to GIA. We find a discrepancy between the observed and modeled rates of between 2.1 and 3.6 mm/yr.Daily values of absolute vertical displacements and fitted terms are displayed in Figure 7.

3.3. Interannual Displacements

[20] During the period 2006–2012, we observe large interannual vertical displacements at all four GPS sites (Figure 8). The largest year-to-year displacements are observed at KAGA (located closest to the front of JI) with a minimum displacement of 16.4 ± 2.3 mm between September 2010 and 2011 and a maximum of 31.7 ± 2.0 mm between September 2011 and 2012. The same pattern, although less pronounced, is observed at all other sites excluding AASI. Here, the maximum uplift is found between September 2009 and 2010. The two periods with the largest year-to-year vertical displacements coincides with the record high surface melting events observed in 2010 and 2012. The year-to-year vertical displacements shown in Figure 8 are obtained by subtracting the mean September vertical displacement for 1 year from the mean September vertical displacement the following year. September is chosen because GPS data from KAGA is available until September 2012 only.

4. Discussion and Conclusions

[21] We have analyzed GPS time series of relative vertical and horizontal displacements from 2006–2012 at the sites KAGA, ILUL, and QEQE to study the regional displacement pattern near JI. In the time span 2006–2010.4, the relative horizontal displacements are all directed towards the north-west. This indicates that the main part of the mass loss occurs southeast of the sites KAGA, ILUL, and QEQE, since the horizontal motion points away from an area with mass loss. This conclusion is consistent with the elevation change grid based on ATM measurements between 2006 and 2010 (Figure 2), where the larger portion of the volume loss is found southeast of the GPS sites. In the time period 2010.4–2012, we observe a decrease in the amplitude of the north components at the sites KAGA and ILUL that indicates increased mass loss to the north of these sites. This interpretation agrees well with the thinning pattern based on ATM data from 2010–2012, in which we observe increased dynamic thinning at the northern glacier arm of JI and increased thinning over a large area just north of the glacier (Figure 2). Hence, our deformation analysis demon-

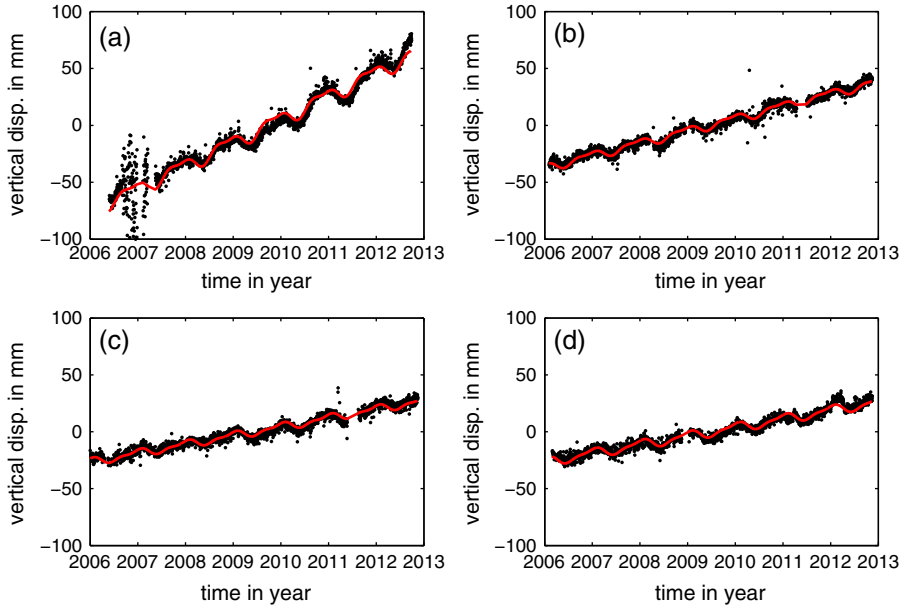

Figure 7. Daily values of vertical displacements at (a) KAGA, (b) ILUL, (c) QEQE, and (d) AASI. The red curves display the best fitting linear, annual, and semi-annual terms based on data from 2006–2012.

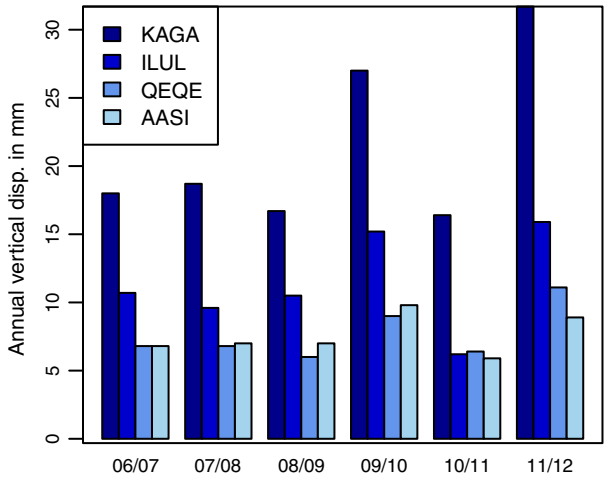

Figure 8. Interannual vertical displacements between Septembers in the period 2006–2012 at the GPS sites KAGA, ILUL, QEQE, and AASI.

strates that we can gain important information about the thinning pattern by considering horizontal displacements. However, caution should be taken with horizontal rates at sites located close to the front since these may be sensitive to mass changes near the front and not the overall mass loss pattern of the glacier.

[22] In the time period 2006–2010.4, the vertical modeled and observed relative rates agree well within the error bars, which suggests that the mass loss signal from JI is well captured. When comparing our modeled vertical rates to those estimated in *Khan et al.* [2010], we have improved the agreement between the observed and modeled rates for both the absolute and the relative displacements. The major difference is our treatment of the mass loss outside JI. In *Khan et al.* [2010], the elastic rates due to mass loss outside JI are derived from a mass balance model based on Gravity Recovery and Climate Experiment (GRACE) data [*Velicogna*, 2009]. Here, we use a high resolution (5×5 km) mass balance model derived from ICESat data. With this model, we obtain a much more detailed mass change pattern than can be obtained with GRACE data. This is important in terms of the elastic displacement in the near field of a GPS receiver since a small disc will produce a larger elastic signal close to the disc compared to that from a larger disc assuming that both discs contain the same mass. This demonstrates the importance of using a high resolution loading model to fully capture the elastic response from nearby sources.

[23] Furthermore, we compare observed and modeled absolute vertical displacement rates for the period 2006–2010.4 where we find a discrepancy of 3.6 mm/yr (KAGA), 2.1 mm/yr (ILUL), 3.2 mm/yr (QEQE), and 2.7 mm/yr (AASI). These discrepancies may originate from various sources such as errors in the elastic rates related to unmodeled mass loss outside JI, errors related to GPS measurements, and errors in the GIA rates owing to inaccuracies in the ice history and viscosity profile. The fact that the offsets are of similar size suggests that the error might be caused by a long wavelength signal, e.g., GIA. For instance, we have demonstrated that the GIA estimates may vary by a few millimeter by varying the viscosity of the upper and lower mantles. Hence, the vertical GIA displacements estimates are not particularly well determined at these sites. The ice history, ICE-5G, used here does not include ice mass changes related to the little ice age (LIA). *Simpson et al.* [2011] predict a viscous response of around ± 0.2 mm/yr due to ice mass changes during the last 100 years that is based on the ice history Huy2 [*Simpson et al*., 2009]. The response may be around ± 1.2 mm/yr for a weak upper mantle. Other studies have demonstrated that the predicted GIA displacement rates vary depending on the ice history used [*Spada et al*., 2012; *King et al*., 2010]. Hence, we might obtain slightly different GIA predictions based on other ice history models such as Huy2 and ANU05 [*Fleming and Lambeck*, 2004]. For instance, the vertical GIA displacement rates based on Huy2 [*Simpson et al.*, 2011] are slightly positive in the area of JI, which will reduce the discrepancy between observed and modeled vertical displacement rates in this analysis.

[24] Furthermore, the ICESat-derived mass change grid, which is used to estimate the displacements rates outside JI, has a shorter time span by 1.4 years than the GPS data. Hence, we might not fully capture the ice mass loss outside JI. This might account for a part of the discrepancy. We estimate this uncertainty to be ± 0.5 mm (section 2.3.2).

[25] When considering interannual vertical displacements at our GPS sites, we find large variations. To determine if these variations are caused by local or regional effects, we compare them with the relative GPS rates (Table 2). We find that the uplift at KAGA is generally dominated by local ice mass loss from JI except for the years 2010 and 2012. In these years, considerably larger uplifts are observed that most likely result from widespread surface melting [*Bevis et al*., 2012]. The fact that we also observe larger uplifts in 2010 and 2012 at the distant sites ILUL, QEQE, and AASI, supports the idea of large scale surface melting since these sites are only affected in a limited sense by potential frontal variations.

[26] This analysis demonstrates that the horizontal motions do contribute additional information about the pattern of ice melt. This additional information can be particularly valuable in areas with a more complex mass loss pattern such as the southeast coast of Greenland where the mass loss results from many different types of glaciers and inland thinning.

[27] **Acknowledgments.** We thank Louise S. Sørensen for providing the ICESat mass change grids and Pascal Gegout for the elastic LDCs and the corresponding elastic Earth model. We would also like to thank the Editor and the reviews for their comments and suggestions, which have improved this manuscript. Work done by Karina Nielsen and Shfaqat Abbas Khan was partly funded by KVUG. GNET is supported by the Arctic Sciences Division of the U.S. National Science Foundation.

References

Altamimi, Z., L. Métivier, and X. Collilieux (2012), ITRF2008 plate motion model, *J. Geophys. Res.*, *117*(B7), B07,402, doi:10.1029/2011JB008930.

Bassin, C., G. Laske, and G. Masters (2000), The current limits of resolution for surface wave tomography in North America, *Eos Trans. Am. Geophys.*, *Un. 81*, F897.

Bevis, M., et al. (2012), Bedrock displacements in Greenland manifest ice mass variations, climate cycles and climate change, *Proc. Natl. Acad. Sci. USA*, *109*, 11944–11948, doi:10.1073/pnas.1204664109.

Böhm, J., B. Werl, and H. Schuh (2006), Troposphere mapping functions for GPS and very long baseline interferometry from European Centre for

medium-range weather forecasts operational analysis data, *J. Geophys. Res.*, *111*(B2), B02,406, doi:10.1029/2005JB003629.

Dietrich, R., A. Rülke, and M. Scheinert (2005), Present-day vertical crustal deformations in West Greenland from repeated GPS observations, *Geophys. J. Int.*, *163*(1-2), 865–874, doi:10.1111/j.1365-246X.2005.02766.X.

Dziewonski, A., and D. Anderson (1981), Preliminary reference Earth model, *Phys. Earth Planet. Inter.*, *25*(4), 297–356.

Farrell, W. (1972), Deformation of the Earth by surface loads, *Rev. Geophys.*, *10*(3), 761–797.

Fleming, K., and K. Lambeck (2004), Constraints on the Greenland Ice Sheet since the Last Glacial Maximum from sea-level observations and glacial-rebound models, *Quat. Sci. Rev.*, *23*, 1053–1107, doi:10.1016/j.quascirev.2003.11.001.

Howat, I. M., Y. Ahn, I. Joughin, M. R. van den Broeke, J. T. M. Lenaerts, and B. Smith (2011), Mass balance of Greenland's three largest outlet glaciers, 2000–2010, *Geophys. Res. Lett.*, *38*, L12,501, doi:10.1029/2011GL047565.

Jacob, T., J. Wahr, W. T. Pfeffer, and S. Swenson (2012), Recent contributions of glaciers and ice caps to sea level rise, *Nature*, *482*, 514–518, doi:10.1038/nature10847.

Khan, S., J. Wahr, L. Stearns, G. Hamilton, T. van Dam, K. Larson, and O. Francis (2007), Elastic uplift in southeast Greenland due to rapid ice mass loss, *Geophys. Res. Lett.*, *34*(21), L21,701, doi:10.1029/2007GL031468.

Khan, S., J. Wahr, E. Leuliette, T. van Dam, K. Larson, and O. Francis (2008), Geodetic measurements of postglacial adjustments in Greenland, *J. Geophys. Res.*, *113*(B2), B02,402, doi:10.1029/2007JB004956.

Khan, S., L. Liu, J. Wahr, I. Howat, I. Joughin, T. van Dam, and K. Fleming (2010), GPS measurements of crustal uplift near Jakobshavn Isbræ due to glacial ice mass loss, *J. Geophys. Res.*, *115*(B9), B09,405, doi:10.1029/2010JB007490.

King, M., et al. (2010), Improved constraints on models of glacial isostatic adjustment: A review of the contribution of ground-based geodetic observations, *Surv. Geophys.*, *31*, 1–43, doi:10.1007/s10712-010-9100-4.

Kouba, J. (2007), Implementation and testing of the gridded Vienna Mapping Function 1 (VMF1), *J. Geodesy*, *82* (4-5), pp. 193–205, doi:10.1007/s00190-007-0170-0.

Krabill, W. B. (2011), IceBridge ATM L2 Icessn elevation, slope, and roughness, [2006–2011], *Boulder, Colorado USA: NASA Distributed Active Archive Center at the National Snow and Ice Data Center. Digital Media*.

Kustowski, B., G. Ekström, and A. Dziewonski (2008), Anisotropic shear-wave velocity structure of the Earth's mantle: A global model, *J. Geophys. Res.*, *113*, B06306, doi:10.1029/2007JB005169.

Nielsen, K., S. A. Khan, N. Korsgaard, K. Kjær, J. Wahr, M. Bevis, L. Stearns, and L. Timm (2012), Crustal uplift due to ice mass variability on Upernavik Isstrøm, west Greenland, *Earth Planet. Sci. Lett.*, *353*, 182–189, doi:10.1016/j.epsl.2012.08.024.

Peltier, W. (2004), Global glacial isostasy and the surface of the ice-age Earth: The ICE-5G (VM2) model and GRACE, *Annu. Rev. Earth Planet. Sci.*, *32*, 111–149, doi:10.1146/annurev.earth.32.082503.144359.

Scherneck, H. G., and M. S. Bos (2002), Ocean tide and atmospheric loading. *IVS 2002 General Meeting Proceedings, Tsukuba, Feb. 4-7, 2002, p. 205-214. NASA Goddard Space Flight Center*, ftp://ivscc.gsfc.nasa.gov/pub/general-meeting/2002/pdf/scherneck.pdf.

Simpson, M., G. Milne, P. Huybrechts, and A. Long (2009), Calibrating a glaciological model of the Greenland ice sheet from the Last Glacial Maximum to present-day using field observations of relative sea level and ice extent, *Quat. Sci. Rev.*, *28*, 1631–1657 , doi:10.1016/j.quascirev.2009.03.004.

Simpson, M., L. Wake, G. Milne, and P. Huybrechts (2011), The influence of decadal-to millennial-scale ice mass changes on present-day vertical land motion in Greenland: Implications for the interpretation of GPS observations, *J. Geophys. Res.*, *116*(B2), B02, 406, doi:10.1029/2010JB007776.

Sørensen, L. S., S. B. Simonsen, K. Nielsen, P. Lucas-Picher, G. Spada, G. Adalgeirsdottir, R. Forsberg, and C. S. Hvidberg (2011), Mass balance of the Greenland ice sheet (2003–2008) from ICESat data—The impact of interpolation, sampling and firn density, *The Cryosphere*, *5*(1), 173–186, doi:10.5194/tc-5-173-2011.

Spada, G. (2003), *The Theory Behind TABOO*, Samizdat Press, Golden-White River Junction.

Spada, G., and P. Stocchi (2007), SELEN: A Fortran 90 program for solving the "sea-level equation", *Comput. Geosci.*, *33*, 538–562, http://dx.doi.org/10.1016/j.cageo.2006.08.006

Spada, G., et al. (2011), A benchmark study for glacial isostatic adjustment codes, *Geophys. J. Int.*, *185*, 106–132, doi:10.1111/j.1365-246X.2011.04952.X.

Spada, G., G. Ruggieri, L. Sørensen, K. Nielsen, D. Melini, and F. Colleoni (2012), Greenland uplift and regional sea level changes from ICESat observations and GIA modelling, *Geophys. J. Int.*, *189*, 1457–1474, doi:10.1111/j.1365-246X.2012.05443.X.

Tedesco, M., X. Fettweis, M. Van den Broeke, R. Van de Wal, C. Smeets, W. van de Berg, M. Serreze, and J. Box (2011), The role of albedo and accumulation in the 2010 melting record in Greenland, *Environ. Res. Lett.*, *6*, 014,005, doi:10.1088/1748-9326/6/1/014005.

Van Den Broeke, M., J. Bamber, J. Ettema, E. Rignot, E. Schrama, W. Van de Berg, E. Van Meijgaard, I. Velicogna, and B. Wouters (2009), Partitioning recent Greenland mass loss, *Science*, *326*(5955), 984–986, doi:10.1126/science.1178176.

Velicogna, I. (2009), Increasing rates of ice mass loss from the Greenland and Antarctic ice sheets revealed by GRACE, *Geophys. Res. Lett.*, *36* (19), L19,503, doi:10.1029/2009GL040222.

Zumberge, J., M. Heflin, D. Jefferson, M. Watkins, and F. Webb (1997), Precise point positioning for the efficient and robust analysis of GPS data from large networks, *J. Geophys. Res.*, *102*(B3), 5005–5017.

Zwally, H., R. Schutz, C. Bentley, J. Bufton, T. Herring, J. Minster, J. Spinhirne, and R. Thomas (2010), GLAS/ICESat L2 Antarctic and Greenland ice sheet altimetry data V031, *National Snow and Ice Data Center, Boulder, CO*.